Subwavelength beam shaping via multiple-metal slits surrounded by slot waveguides

Sen Jia, Jinhai Si*, Lihe Yan, Feng Chen, Xun Hou

Key Laboratory for Physical Electronics and Devices of the Ministry of Education & Shaanxi Key Lab of Information Photonic Technique, School of Electronics & Information Engineering, Xi'an Jiaotong University, Xianning-Xilu 28, Xi'an 710049, China

ARTICLE INFO

ABSTRACT

We design a novel plasmonic lens consisting of multiple nano-metal slits surrounded by dielectric air slot waveguides. The surface plasmon polaritons (SPPs) are excited from the metal slits. The slot waveguides provide desired phase retardations of light focusing. Numerical simulations with finite-difference time-domain (FDTD) method show that the transmitted fields through the design example can generate light focusing and deflection by altering the width or length of slot waveguides. The focal spot size is far narrower than the incident wavelength and the focal length can be controlled in several micrometers, which agree with our theoretical analysis.

© 2012 Elsevier B.V. All rights reserved.

1. Introduction

Surface plasmon polaritons (SPPs) are propagating electromagnetic surface modes bounded along metal–dielectric interfaces. The most attractive feature of SPPs is its potential for developing nanoscale optical devices that have the ability to manipulate light on a subwavelength scale [1–6]. Previously, various kinds of plasmonic optical devices, including all optical switch, narrow-band filter, demultiplexer, interferometer, splitter, plasmonic lens and waveguide [7–16], have been proposed to manipulate optical signals in the nanoscale. Furthermore, in the terahertz (THz) region, an active THz plasmonic device has also been designed to implement beam focusing [17]. As a fundamental component of plasmonic circuits, plasmonic lenses have been the focus of many studies. Many kinds of metal-based plasmonic lens have been proposed and validated using both numerical simulations and experiments [18–25]. In these designs, various nano-structures, such as slits with variant depths [18] or widths [19], single slit surrounded with grooves [20,21], are fabricated on thin metallic film to implement the beam focusing. However, during the deposition process, metal has a tendency to crystallize which makes it very difficult to obtain the desired perfect shape during fabrication by using a focused ion beam (FIB) [26,27]. To overcome this deficiency, another effective way of realizing subwavelength focusing is the use of composite structure composed of metal–dielectric. Representatively, Kim et al. proposed an ingenious structure for light focusing and deflection by a single subwavelength metal slit surrounded by chirped dielectric surface gratings [22]. In this structure, the directions of the radiation fields from surface gratings are determined by the resonance property of gratings. Therefore, adjusting the resonance property of each grating by changing the grating period could make those radiated fields with different directionalities converge toward an expected point. However, such design could only be used in the structure with a single metal slit, and the spot size generated from the structure is smaller than the input wavelength.

In this paper, we present a novel plasmonic lens based on composite structure to realize the subwavelength optical focusing. In the structure, multiple nano-metal slits are surrounded by a dielectric air slot waveguide array at the exit surface of metal. The SPPs are excited from the metal slits. The dielectric slot waveguides with variant widths or lengths provide desired phase retardations of beam manipulation. Thus, the metal slits could be fabricated with fixed widths, depths and interspaces. According to this design principle, two phenomena, beam deflection and focus, are numerically studied using the finite-difference time-domain (FDTD) method. The simulation results show that the focal spot size is closer to the diffraction limit.

2. Principle

The dielectric slot waveguide can confine light to the subwavelength level. Fig. 1(a) shows a schematic of the slot waveguide

* Corresponding author.
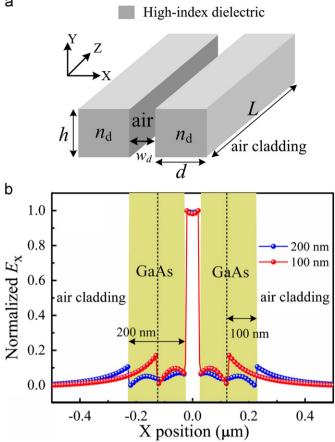   E-mail address: jinhaisi@mail.xjtu.edu.cn (J. Si).

Fig. 1. (a) Schematic of the slot waveguide structure and (b) Transverse electric field of the *TM* mode in a dielectric air slot waveguide, when w_d=50 nm, n_d=3.664, n_S=1, and n_C=1.

structure, where a nanometer-wide low-index slot is embedded between two rectangular high-index regions, both surrounded by a low-index cladding. The principle of the slot waveguide is based on the discontinuity of the normal component of the electric field at the high index-contrast interface [28]. This discontinuity can be used to strongly confine light in a nanometer-wide region of low-index material. The feature of slot waveguide has been both in the theoretical analysis and experiments [28,29]. For our investigations, the electric field E and magnetic field H of incident transverse magnetic (*TM* polarization) waves are defined along the x and y directions, respectively. The coordinate system is shown in Fig. 1(a). As the component of the electric field (Ex) of the *TM* wave is perpendicular to high-index regions, it undergoes strong discontinuity at the high index-contrast interface, with much higher amplitude in the low-index regions. Fig. 1(b) shows the transverse electric field distribution of the 800 nm TM mode in a dielectric air slot waveguide with a 50 nm slot aperture and 100 nm or 200 nm individual dielectric wall. Here, gallium arsenide (GaAs) has been chosen as the wall material of slot waveguide because of its high refractive index. The refractive index of GaAs is 3.664 at 800 nm [30]. The slot region and the cladding are filled with air and the refractive index is 1. From Fig. 1(b), one can clearly see the electric field discontinuities at index-contrast interfaces which concentrate strongly in the air slot region. This character enables it to be easily compatible with other nanometer photonic devices as integrated optical component.

When incident light from the bottom of the slab with 800 nm wavelength is coupled to SPP modes at the entrance of the metallic slits, radiating fields occur at the ends of metallic slits

with the initial phase retardations from Eq. (1) [19].

$$\tanh\left(\frac{w}{2}\sqrt{\beta^2-k_0^2\varepsilon_d}\right)=\frac{-\varepsilon_d\sqrt{\beta^2-k_0^2\varepsilon_m}}{\varepsilon_m\sqrt{\beta^2-k_0^2\varepsilon_d}} \quad (1)$$

where k_0 is the wave vector of light in free space, ε_m and ε_d are the relative dielectric constants for the metal and the materials between slits, and w is the slit width. The imaginary part of β represents the decibel loss coefficient per unit length, which is usually ignorable for light propagation in short metal slit. The value of Re(β/k_0) represents the effective refractive index in the slit and determines the phase retardation. Fig. 2(a) plots the Re(β/k_0) value of SPPs wave in the metal slit for variant width. The metal assumed is silver. The complex relative permittivity of silver at 800 nm wavelength is characterized by the Drude model:

$$\varepsilon_m(\omega)=\varepsilon_\infty-\frac{\omega_p^2}{\omega(\omega+i\gamma)} \quad (2)$$

where ε_∞ stands for the dielectric constant at the infinite frequency, ω_p and γ are the natural frequency of the oscillations of free conduction electrons and damping frequency of the oscillations, ω is angular frequency of incident light. The parameters for silver can be set as ε_∞=3.7, ω_p=9.1 eV, γ=0.018 eV [31]. The dielectric
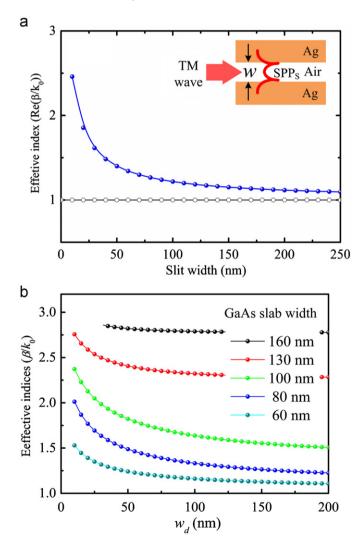

Fig. 2. (a) The effective indices for different slit widths using silver at a wavelength of 800 nm. The dotted line represents the value in air. The inset shows the schematic diagram of the Ag–air–Ag plasmonic waveguide structure and (b) The effective indices versus slot aperture w_d and individual slot wall width d.

constant of air is $\varepsilon_d = 1$. As shown in Fig. 2(a), the value of $Re(\beta/k_0)$ decreases rapidly with increased slit widths but drops steadily for slit widths below about 50 nm. Due to the surface wave property, $Re(\beta/k_0)$ is always above the white dotted line which stands for the light in air.

On the other hand, when the SPPs mode is propagating in the slot waveguide, the propagation constants β of SPPs mode can be calculated by solving the equation [28]:

$$\tan\left(H\sqrt{k_0^2 n_H^2 - \beta^2} - \theta\right) = \frac{n_H^2}{n_S^2} \frac{\sqrt{\beta^2 - k_0^2 n_S^2}}{\sqrt{k_0^2 n_H^2 - \beta^2}} \tanh\left(\frac{w_d}{2}\sqrt{\beta^2 - k_0^2 n_S^2}\right) \quad (3)$$

$$\theta = \arctan\left(\frac{n_H^2}{n_C^2} \frac{\sqrt{\beta^2 - k_0^2 n_C^2}}{\sqrt{k_0^2 n_H^2 - \beta^2}}\right) \quad (4)$$
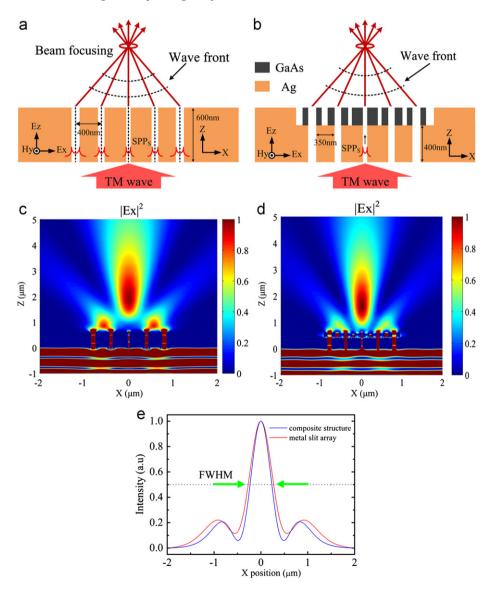
where n_S, n_C and n_H stand for the indices of air slot region, air cladding, and GaAs wall, respectively. H and w are the widths of the dielectric wall and air slot, respectively. Fig. 2(b) shows the dependence of effective index (β/k_0) versus slot aperture w_d and individual wall width H, respectively. As shown in the figure, the propagation constant of the slot waveguide depends greatly on the width of the waveguide wall and slot aperture. Therefore, SPPs wave passing through dielectric air slot waveguides with different parameters will experience different phase retardations. If this character is utilized appropriately, the phase of the light transmitted through the slot waveguides can be controlled in order to produce light focusing and deflection.

3. Simulation and discussion

To demonstrate the validity of the design, two-dimensional FDTD method is employed. Perfect matched layer (PML) absorbing boundary conditions are used at all boundaries. In the FDTD algorithm, the spatial grid sizes in the x and the z directions are chosen to be 5 nm × 5 nm. The wavelength of incident TM polarized monochromatic plane wave is 800 nm in air.

For comparison, simulation of only plasmonic lens based metal slits is also performed. Fig. 3(a) and (b) shows the schematic geometries of a metal slit array and a composite structure investigated in this work, respectively. For the plasmonic lens based metal slits only, the geometrical parameters are designed as follows: the thickness of silver film is 600 nm, the slit width in

Fig. 3. The schematics of beam focusing structures (a) metal slits with variant widths. (b) composite structure. The normalized intensity distribution of the focused beam from (c) the metal slits with variant widths and (d) the composite structure. (e) Cross-sections plot at the focal planes.
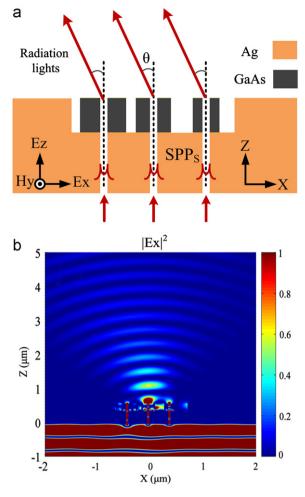
the five-slit array is 110, 80, 50, 80 and 110 nm from left to right, the distance between two slits is 400 nm (center to center). For the composite structure, a central strip is fabricated on an Ag film. The depth and width of the strip are 200 nm and 2.2 μm, respectively. The GaAs slot waveguides are fabricated on the exit surface of slits and the wall widths are 85, 120, 155, 120 and 85 nm from left to right. This configuration could help to decrease device dimension and avoid slot waveguide damage. The other parameters are the same as those used in Fig. 3(a).

Fig. 3(c) and (d) compares the field intensity distribution of the metal slits array only and the metal slits surrounded by slot waveguides. Here, the time-average electric-field intensity $|Ex|^2$ is used to represent field intensity distribution. The full widths at half-maximums (FWHMs) of focal spots are 545 nm and 463 nm for the two structures, respectively. Fig. 3(e) also shows the intensity patterns along the x direction through the foci of two structures. Clearly, compared with the metal slits structure, the focal spot of the composite structure shows a significant FWHM reduction as much as 15%, close to half the input wavelength. Further, as shown in Fig. 2(b), we note the fact that phase retardation enough to generate light focusing can be achieved by only adjusting the parameters of slot waveguide appropriately. It means that the metal slits can have equal width, interspaces, and depth, which will reduce greatly the fabrication difficulty and configuration complexity.

We first demonstrate beam deflection using such a composite structure. Fig. 4(a) shows the schematic diagram of a three-slit composite structure. The depth and width of the central strip are 200 nm and 1.5 μm, respectively. Metal slits with an equal width of 50 nm are fabricated on the strip and the interspacing between adjacent slits is 400 nm (center to center). The widths of slot waveguide are 180 nm, 100 nm and 70 nm in sequence from left to right. When the input wave is incident to the bottom side of the slit array, the SPPs are excited from the metal slits and propagate along the metal slits in a waveguide mode. Because of the metal slits with equal width and depth, the difference of phase retardations between slits is not generated when the SPPs are propagating at metal slits zone. However, when the SPPs arrive at slot waveguide zone, the different waveguide widths would introduce difference phase retardation among the radiation components at the exit surface of slot wavelengths and result in beam deflection. As illustrated in Fig. 4(b), the simulation results clearly reveal that the transmitted beam propagates along the direction tilted toward the wider side of slot wavelength. A main beam deflection of ~8° can be observed.

According to the same principle, a plasmonic lens is designed. Fig. 5(a) shows the schematic of proposed structure. In this focusing scheme, five metal slits are surrounded by dielectric air slot waveguides at the exit of slits. The width of the central strip is 1.5 μm. The widths of waveguide wall are 115, 130, 160, 130 and 115 nm from left to right, respectively. The other parameters are the same as those used in Fig. 4(a). Fig. 5(b) shows the distributions of the transmitted field intensity for the proposed structure. The FWHM at focal plane is 681 nm. Although this design can realize subwavelength focusing, the spot size is only slightly less than the input wavelength. Therefore, it is absolutely essential to optimize the configuration to obtain better focusing properties.

In previous work [15], metal slits with variant width are used to generate different phase retardations when light transmits through them, which can be utilized to implement beam focusing. Considering the fact that the slot waveguide can produce a high degree of optical confinement in the air core, this is very similar to the metal slit. Therefore, the same principle may also apply to the slot waveguide. We also expect to manipulate the SPPs mode by inducing different phase retardations when they transmit through the slot waveguides with variant lengths.
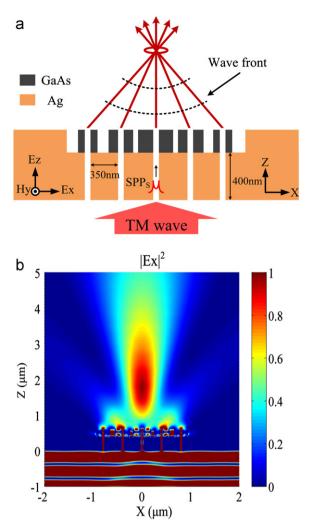

Fig. 4. (a) A schematic drawing of a three-slit composite structure for beam deflection and (b) The simulation results of beam deflection.
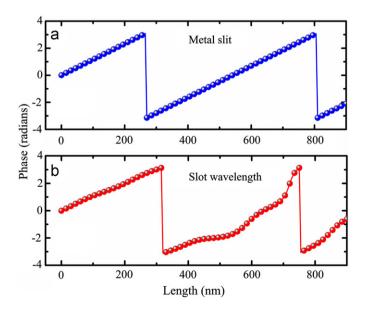
As shown in Fig. 6(a), FDTD simulation result indicates that the phase delay at the metal slit exit increased steadily with the increasing slit length at the start, and when the metal slit became lengthier, it varies periodically with the metal slit length at a period of 520 nm. Similarly, for slot waveguide, the phase delay also varies periodically with the waveguide length at a period of 450 nm. Obviously, this suggests an effective method to modulate the output beam by means of varying the slot waveguide length distribution profile.

Fig. 7(a) shows the schematic diagram of a three-slit composite structure for beam deflection. A central strip is fabricated on an Ag film with 600 nm thickness and filled with GaAs. The depth and width of the strip are 200 nm and 950 nm, respectively. Metal slits are fabricated on the strip and the interspacing between adjacent slits is 250 nm (center to center), which is much larger than the skin depth of surface plasmon inside the silver [32]. The metal slit width is 50 nm. The thickness of GaAs layer is varied with a fixed step profile such that the slot waveguide lengths also change in sequence. In Fig. 3(b), the simulation result clearly reveals that the transmitted beam propagates along the direction tilted toward the longer side of slot wavelength. A main beam deflection of ~28° can be observed and the corresponding GaAs thickness is varied with a 60 nm step profile.
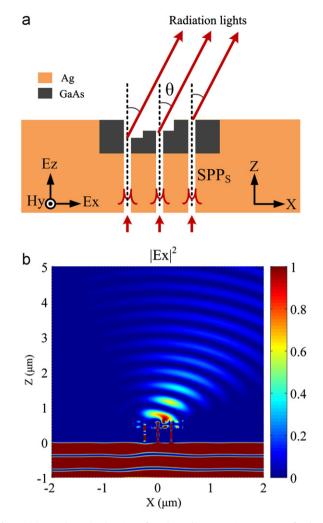
Based on the same principle, the beam focusing can also be performed using a composite structure. Fig. 8(a) shows the schematic diagram of the focusing design. Seven metal slits are surrounded by a slot waveguide array on the output metal

Fig. 5. (a) The schematic of beam focusing structure and (b) The intensity time-average distribution of the focused beam.
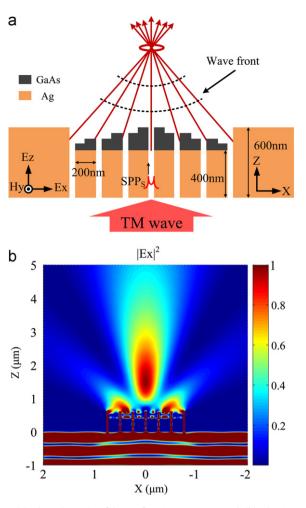

Fig. 7. (a) A schematic drawing of a three-slit composite structure for beam deflection and (b) The simulation result of optical transmission through the structure.

surface. For simplicity the design, the outermost dielectric gratings are replaced by metallic corners. The width of the central strip is 1.55 μm and the other parameters are the same as those used in Fig. 7(a). Fig. 8(b) shows the corresponding intensity distributions. The generated focal length is 1.125 μm, and FWHM at focal plane is 508 nm. In this focusing structure, because the slot waveguide is capable of strongly confining light in the air core region (see Fig. 1(b)), the confined light cannot propagate to the two metallic corners and are reflected by them. As a result, although a part of light passing through the two outermost slits can be reflected toward the focus spot by the corners, most of the light in the focal region comes from slot waveguides. Therefore, the principal cause of forming a beam focus is the phase delay caused by the slot waveguides rather than the reflection from the metallic corners.

4. Conclusion

In summary, a plasmonic lens composed of metal nano-slits surrounded by dielectric slot waveguides is proposed. Two main phenomena, optical beam deflection and focusing, are investigated numerically. The simulation results clearly show that the deflection angle and the focal spot size can be controlled by adjusting the parameters of slot waveguides. The focal spot can be far smaller than the incident wavelength. Such a plasmonic lens

Fig. 6. FDTD simulation results of relative phase at the center of the exit as a function of the waveguide length (a) metal slit and (b) slot waveguide. The width of these both are assumed to be 50 nm.

Fig. 8. (a) The schematic of beam focusing structure and (b) The intensity distribution of the focused beam. The slot waveguide length is varied with a 20 nm step profile.

has great potential applications in integrate optics, data storage, and optical sensors.

Acknowledgments

References

[1] T.W. Ebbesen, H.J. Lezec, H.F. Ghaemi, T. Thio, P.A. Wolff, Nature 391 (1998) 667.
[2] H.F. Ghaemi, T. Thio, D.E. Grupp, T.W. Ebbesen, H.J. Lezec, Physical Review B 58 (1998) 6779.
[3] N. Fang, H. Lee, C. Sun, X. Zhang, Science 308 (2005) 534.
[4] H.J. Lezec, A. Degiron, E. Devaux, R.A. Linke, F. Martin-Moreno, L.J. Garcia-Vidal, T.W. Ebbesen, Science 297 (2002) 220.
[5] W.L. Barnes, A. Dereux, T.W. Ebbesen, Nature 424 (2003) 824.
[6] L.B. Yu, D.Z. Lin, Y.C. Chen, Y.C. Chang, K.T. Huang, J.W. Liaw, J.T. Yeh, J.M. Liu, C.S. Yeh, C.K. Lee, Physical Review B 71 (2005) 041405.
[7] C. Min, P. Wang, C. Chen, Y. Deng, Y. Lu, H. Ming, T. Ning, Y. Zhou, G. Yang, Optics Letters 33 (2008) 869.
[8] C. Min, G. Veronis, Optics Express 17 (2009) 10757.
[9] J. Tao, X.G. Huang, X.S. Lin, Q. Zhang, X. Jin, Optics Express 17 (2009) 13989.
[10] J. Tao, X. Huang, J. Zhu, Optics Express 18 (2010) 11111.
[11] Z. Han, L. Liu, E. Forsberg, Optics Communications 259 (2006) 690.
[12] S. Passinger, A. Seidel, C. Ohrt, C. Reinhardt, A. Stepanov, R. Kiyan, B. Chichkov, Optics Express 16 (2008) 14369.
[13] L. Wang, S.M. Uppuluri, E.X. Jin, X.F. Xu, Nano Letters 6 (2006) 361.
[14] T. Lee, S. Gray, Optics Express. 13 (2005) 9652.
[15] G. Veronis, S. Fan, Applied Physics Letters 87 (2005) 131102.
[16] J.L. Liu, H.F. Zhao, Y. Zhang, S.T. Liu, Applied Physics B 98 (2010) 797.
[17] B. Hu, Q.J. Wang, S.W. Kok, Y. Zhang, Plasmonics (published online, 2011). "Active focal length control of terahertz slitted plane lenses by magneto-plasmons," Plasmonics (published online, November 2, 2011).
[18] Z.J. Sun, H.K. Kim, Applied Physics Letters 85 (2004) 642.
[19] H.F. Shi, C.T. Wang, C.L. Du, X.G. Luo, X.C. Dong, H.T. Gao, Optics Express 13 (2005) 6815.
[20] H.F. Shi, C.L. Du, X.G. Luo, Applied Physics Letters 91 (2007) 093111.
[21] Fenghua Hao, Rui Wang, Jia Wang, Optics Express 18 (2010) 15741.
[22] S. Kim, Y. Lim, H. Kim, J. Park, B. Lee, Applied Physics Letters 92 (2008) 013103.
[23] Z.W. Liu, J.M. Steele, W. Srituravanich, Y. Pikus, C. Sun, and X. Zhang, Nano Letters 5 (2005) 1726.
[24] L. Yin, V.K. Vlasko-Vlasov, J. Pearson, J.M. Hiller, J. Hua, U. Welp, D.E. Brown, C.W. Kimball, Nano Letters 5 (2005) 1399.
[25] L. Verslegers, P.B. Catrysse, Z. Yu, S. Fan, Physical Review Letters 103 (2009) 033902.
[26] L.B. Yu, D.Z. Lin, Y.C. Chen, Y.C. Chang, K.T. Huang, J.W. Liaw, J.T. Yeh, J.M. Liu, C.S. Yeh, C.K. Lee, Physical Review B 71 (2005) 041405.
[27] D.Z. Lin, C.K. Chang, Y.C. Chen, D.L. Yang, M.W. Lin, J.T. Yeh, J.M. Liu, C.H. Kuan, C.S. Yeh, C.K.D. Lee, Optics Express 14 (2006) 3503.
[28] V. Almeida, Q. Xu, C.A. Barrios, M. Lipson, Optics Letters 29 (2004) 1209.
[29] Q.F. Xu, V.R. Almeida, R.R. Panepucci, and M. Lipson, Optics Letters 29 (2004) 1626.
[30] S. Zollner, Journal of Applied Physics 90 (2001) 515.
[31] J. Park, H. Kim, B. Lee, Optics Express 16 (2008) 413.
[32] M. Scalora, M.J. Bloemer, A.S. Pethel, J.P. Dowling, C.M. Bowden, A.S. Manka, Journal of Applied Physics 83 (1998) 2377.